Journal of Structural Geology, Vol. 9, No. 8, pp. 1021 to 1028, 1987
Printed in Great Britain

0191-8141/87 $03.00 + 0.00

The determination of 'buckling rotation' and its application to theoretical and experimental models of buckle folds

NOELLE ODLING*

P.R.U., Department of Geology, University of Cape Town, Private Bag, Rondebosch, Cape Province, South Africa

(*Received* 24 *January* 1986; *accepted in revised form* 29 *April* 1987)

Abstract—The quantity 'buckling rotation' is defined, for buckle folds, as the total rotation of a fold limb minus the rotation that would occur due to pure shear if no competence contrast existed. Using existing models (theoretical and experimental) of buckle-fold development, the quantity 'buckling rotation' has been calculated for successive small increments of strain and plotted against strain or limb dip. The resulting curves are skewed and bell-shaped, indicating an initial sharp increase in buckling rotation early in fold development followed by a gentle, asymptotic decrease. The curve height and position are dependent on the competence contrast and, in multilayer systems, on the ratio of competent to incompetent layer thickness. The initial sharp increase in buckling rotation corresponds to the period of most active layer-parallel shortening during fold development.

INTRODUCTION

EXPERIMENTAL and theoretical studies of buckle folding since the 1950's have included theoretical and experimental investigations of low-amplitude folding, dominant wavelengths, fold shapes and stress and strain distributions of both single-layer and multilayer systems (e.g. Biot 1957, Chapple 1968, Ramberg 1964). More recently, finite-element analysis has been applied to the simulation of buckle-fold development for a wide range of material properties (e.g. Dieterich & Carter 1969). These methods have shed light on many aspects of buckle folding such as the initiation and early development of folds, the effects of various material properties and viscosities of the layer and its matrix, and the change in shape with associated stress and strain distributions during fold growth. The present paper investigates a single aspect of buckle folding; the rotation of the fold limb during fold growth, incorporating the relevant results from some of these studies.

The deformation at any point during buckle folding may be thought of as many small increments of simultaneous pure shear and rigid-body rotation. In the simplest approach, both components are constant for each deformation increment, a model discussed by Hudleston & Stephansson (1973). However, such a model meets problems at high strains. This is illustrated by the case of a layer which buckles due to compression parallel to the initial orientation of the layer. In such a case, constant rotation per deformation increment will result in the fold limbs rotating through each other when the fold has attained an isoclinal form. This is clearly not possible and thus the rotation component must vary during fold development. A method of determining the variable increment, here termed 'buckling rotation' from existing data on fold growth, is described below.

* Present address: I.K.U., Håkon Magnussons Gate 1B, P.O. Boks 1883, Jarlesletta, 7001 Trondheim, Norway.

DETERMINATION OF BUCKLING ROTATION

When a layer which has a different competence from its matrix is shortened in a direction parallel to the layer, it responds by buckling and folds develop. Once a fold has formed, the fold limbs lie at an angle to the bulk-shortening direction and further rotation can be broken down into two components: (a) the rotation which would occur due to pure shear if no competence contrast existed; and (b) the additional rotation due to the buckling of the layer (Fig. 1a). Both components add up to give the total rotation of the layer. In the two-dimensional case, the rotation of a passive layer due to pure shear can be calculated for a small increment of deformation using equation 3-34 of Ramsay (1967);

$$\tan \theta' = \tan \theta(\lambda_1/\lambda_2)^{0.5},$$

where θ is the angle of dip of the layer to the shortening direction (λ_2) prior to deformation, θ' is the angle of dip of the layer after deformation, and λ_1, λ_2 are the principal quadratic elongations of the deformation increment.

By subtracting this 'pure shear' dip from the actual dip of the layer after successive equal increments of bulk-shortening strain, the 'buckling rotation' values can be calculated, and its variation throughout the strain history documented. Figure 1(b) shows an example of the total rotation per increment of bulk-shortening strain separated into 'pure shear rotation' and 'buckling rotation', against bulk strain, calculated for a buckle-fold model from Shimamoto & Hara (1976). The sum of the 'pure shear' and 'buckling rotation' components is the total rotation for each increment. The total rotation and buckling rotation components show an initial sharp increase followed by a gradual decrease with bulk strain while the pure shear rotation shows lower values, increasing more gradually to a maximum at strains that correspond to a limb dip of 45° (in this case 38% ε_s); the maximum value depends on the size of the bulk-shortening increment chosen (2% ε_s here).

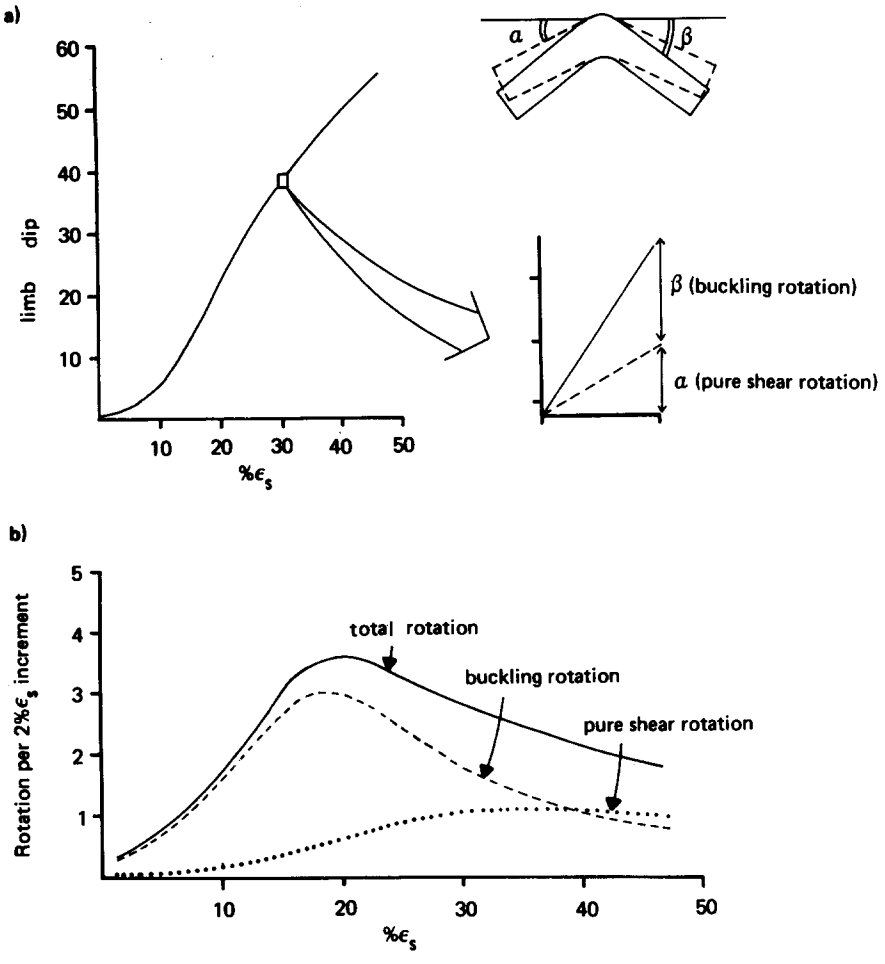

Fig. 1. (a) For each small segment of the strain vs limb dip curve, the rotation that would occur due to pure shear if no competence contrast existed (α) can be calculated. The difference between this and the total rotation for this segment is the additional rotation due to buckling, here termed 'buckling rotation' (β). (b) Plots showing the variation in total, 'pure shear' and 'buckling rotation' per 2% ε_s increment of strain with respect to strain for a single-layer buckle fold model (viscosity ratio 100) from Shimamoto & Hara (1976).

For any strain increment, the 'pure shear rotation' component corresponds to the rotation occurring when no competence contrast exists between the layer and its matrix and is therefore the minimum possible value for the total rotation. The quantity 'buckling rotation' therefore represents the rotation over and above this minimum value. Figure 1(b) shows that the 'pure shear rotation' component is itself variable with strain and thus, by using this component as a base the rotational behaviour of a buckle-fold limb may be compared to that of a passive layer.

The above method has been applied to three finite-element studies and one experimental study of fold growth from the literature. The finite-element models for single layers are from Shimamoto & Hara (1976) and Hudleston & Stephansson (1973), and for multilayers from Williams (1980). In these two-dimensional models, the layer has the form of a low-amplitude fold (necessary to initiate folding in the models) with the axial trace perpendicular to the principal compressive stress direction. For a more detailed account of the finite-element method, the reader is referred to the above authors.

The experimental model of single-layer buckle folds is from Hudleston (1973). The layer is embedded in a material of differing viscosity, with the maximum compressive stress applied parallel to the layer. Plane-strain deformation is imposed, thus preserving area within the study plane. The treatment is therefore two-dimensional and the results can be compared with those of the above finite-element models. In this experimental model, the naturally occurring irregularities of the layer surface were allowed to initiate the folding process.

In all models, the quantity 'limb dip' refers to the maximum angle between the layer and the maximum compressive stress direction and thus refers to the dip at the limb inflexion point, the fastest rotating part of the layer. The variation in limb dip with respect to strain is recorded in graphical form by Hudleston & Stephansson (1973, fig. 7), Shimamoto & Hara (1976, fig. 3), Williams (1980, fig. 7) and in numerical form by Hudleston (1973, fig. 3). For the purposes of comparison, percentage shortening, the unit of strain used by Hudleston and Stephansson (1973) and Hudleston (1973), has been converted to natural strain (% ε_s) used by Shimamoto & Hara (1976) and Williams (1980). Buckling rotation values have been calculated for 2% ε_s increments of strain throughout.

THE VARIATION OF BUCKLING ROTATION WITH STRAIN IN MODEL FOLDS

The finite-element models of Shimamoto & Hara (1976) and Hudleston & Stephansson (1973) simulate the growth of a low amplitude fold with the dominant wavelength (i.e. the fastest growing fold wavelength at low amplitudes, Biot 1957). Shimamoto & Hara (1976) produced models at viscosity ratios of layer to matrix of 100, 50, 30 and 10 with initial fold limb dips of 1, 4 and 10°. Hudleston & Stephansson (1973) modelled folds in layers with viscosity ratios of 1000, 100, 10 and 1, all models having an initial limb dip of 3°. From the graphs of limb dip vs strain, buckling rotation vs strain curves have been constructed and these are shown in Figs. 2 and 3.

All models give skewed, bell-shaped curves (Figs. 2 and 3), indicating that buckling rotation increases sharply with bulk strain in the early stages of folding and then decreases with approximately exponential decay as the limb dip approaches high angles (i.e. as the fold tends towards isoclinal). The higher the viscosity ratio between the layer and its medium, the greater the maximum value of buckling rotation and the more markedly skewed the curve. This is in agreement with the observation of Shimamoto & Hara (1976) that fold growth is initially rapid, but decreases in the later stages, and that the rate of fold growth is lower for decreasing viscosity ratios. Thus, for a viscosity ratio of 1000 (Hudleston & Stephansson, 1973), a large maximum buckling rotation value is reached within the first 2% ε_s strain increment, whereas for viscosity ratios of 10, maximum buckling rotation values are low and occur at strain values of around 30–40% ε_s.

In Fig. 2(b), the plots for models using initial limb dips of 4 and 10° are superimposed so that their limb dips correspond, using the case of initial limb dip 1° as a reference curve. The buckling rotation vs strain curves

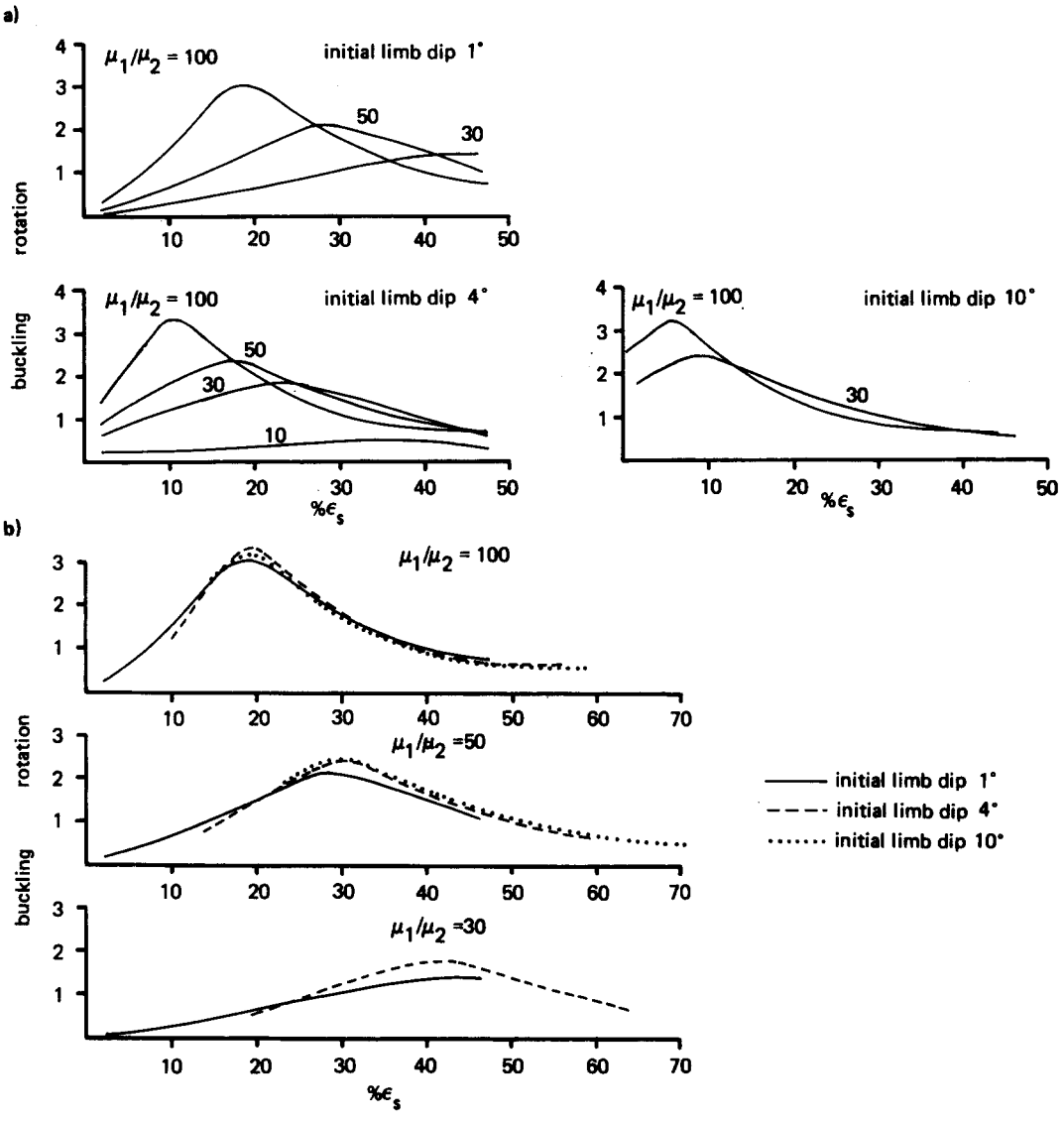

Fig. 2. Curves of buckling rotation vs bulk strain constructed from data from the finite-element single-layer fold models of Shimamoto & Hara (1976). The models were initiated with low-amplitude folds of dominant wavelength. (a) All models show skewed, bell-shaped curves in which the maximum value of buckling rotation and the skewness increase with viscosity ratio (μ_1/μ_2). The effect of increasing the initial limb dip is to shift the curves to the left. (b) For each viscosity ratio, the curves of initial limb dip 4 and 10° have been superimposed on that of initial limb 1°. The curves show good agreement.

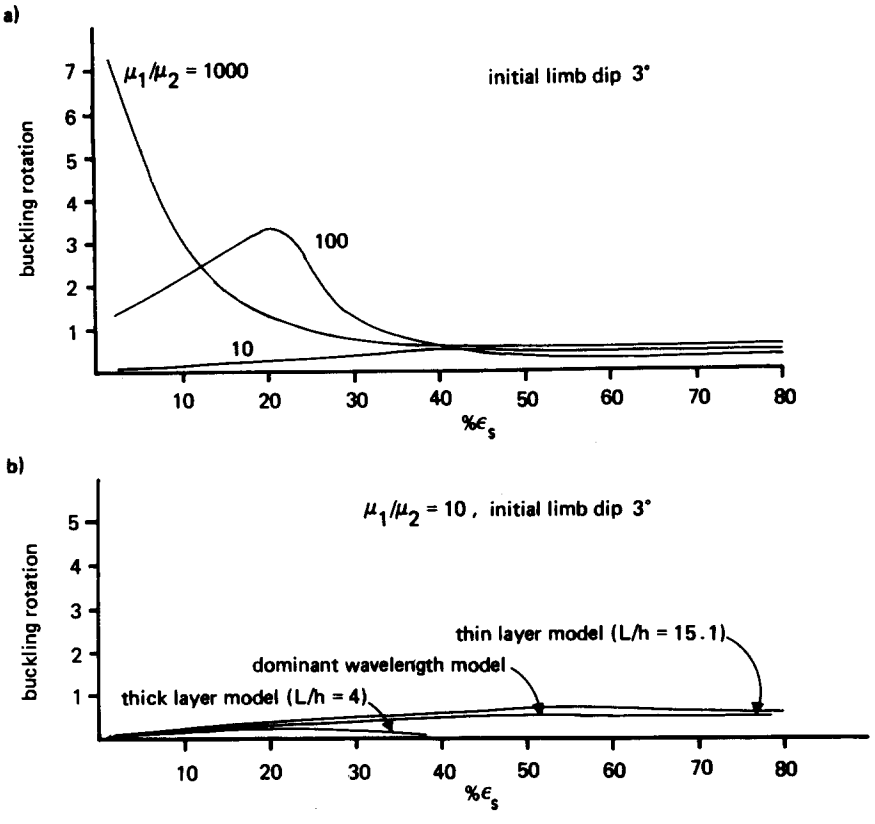

Fig. 3. Curves of buckling rotation vs bulk strain for the finite-element single-layer models of Hudleston & Stephansson (1973). (a) Curves for models in which the initial fold, of limb dip 3°, was of dominant wavelength for each of the viscosity ratios modelled. (b) Curves for three models of viscosity ratio 10, showing the effects of varying layer thickness for a constant wavelength. The thinner layer shows increased, and the thicker layer decreased, buckling activity with respect to the dominant wavelength model.

show good agreement although there is a slight tendency for higher initial limb dip models to reach higher buckling rotation values.

Hudleston & Stephansson (1973) modelled the effects of varying layer thickness (h) for a constant viscosity ratio (μ_1/μ_2 = 10) and wavelength (L) and the resulting buckling rotation vs strain curves are shown in Fig. 3(b). The thinner layer (L/h = 15.1) shows a slight increase in buckling rotation and the thicker layer (L/h = 4.0) a reduced buckling rotation, compared to the dominant wavelength model (L/h = 7.4). This is in agreement with Hudleston and Stephansson's observation that the thinner layer behaves in the most competent, and the thicker layer in the least competent fashion.

The finite-element analyses are compared to the experimental models of single-layer folds of Hudleston (1973). In these experiments, solutions of ethyl cellulose in benzyl alcohol, the behaviour of which closely approximates viscous flow during deformation, were used. Hudleston found that the effects of diffusion significantly reduced the ideal viscosity ratios and so apparent viscosity ratios were calculated using the wavelength/thickness ratios of the folds produced. The buckling rotation vs strain curves for the experimental models are shown in Fig. 4. The curves from the experimental models show similar forms to those derived from the finite-element models; that is, skewed, bell-shaped curves whose maxima decrease and migrate to the right with decreasing viscosity ratio of layer to matrix.

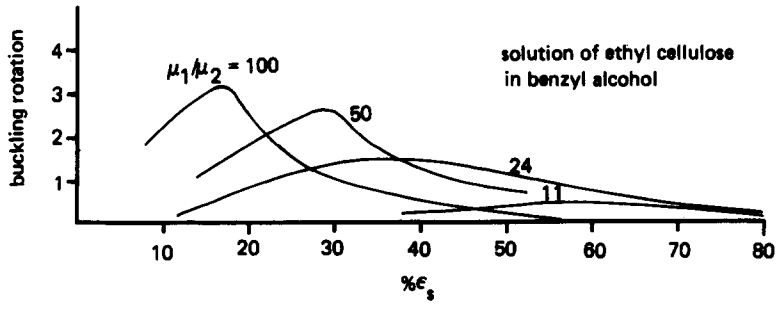

Fig. 4. Curves of buckling rotation vs bulk strain for experimental models of single-layer buckle folds, from Hudleston (1973). Natural irregularities in the layer surface were used to initiate folding.

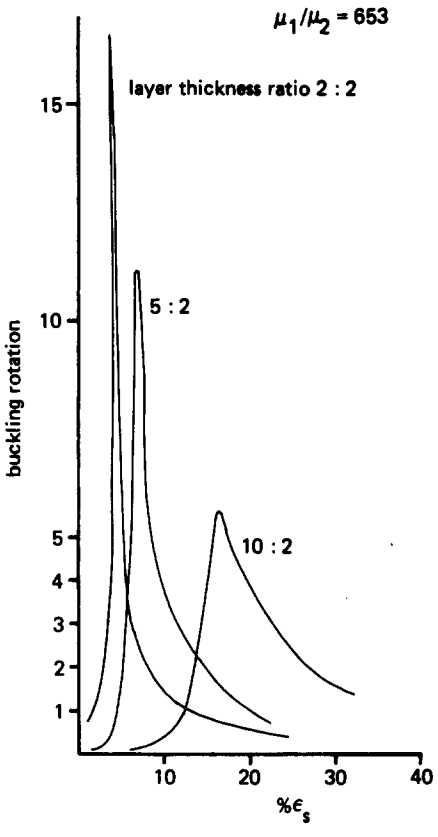

Fig. 5. Curves of buckling rotation vs bulk strain for the finite-element multilayer models of Williams (1980). The curves show the same general form (skewed, bell-shaped) as those for single-layer models. The viscosity ratio is kept constant (653) and the thickness ratio (competent : incompetent) of the layers varied, as labelled. Maximum values of buckling rotation and curve skewness increase with decreasing thickness ratio.

The growth of folds in the interior region of a multilayer complex composed of a regular sequence of competent and incompetent layers, has been studied by Williams (1980) using finite-element methods. In these models, the geometry of each competent layer is constrained by its neighbours to a similar style (Williams 1980). Three models comprising different ratios of competent to incompetent layer thickness, each with a viscosity contrast of 653, are studied here. Buckling rotation vs strain curves, calculated from the models, are shown in Fig. 5. A similar pattern to the single-layer models, that of a skewed, bell-shaped curve, is produced by the multilayered models. Since the viscosity ratio is constant, the variation in maximum buckling rotation and skewness are here related to the thickness ratio between the competent and incompetent layers. Models composed of layers of equal thickness show the most extreme skewness and greatest value of buckling rotation and these factors decrease as the thickness ratio (competent : incompetent) increases.

COMPARISON OF MODELS

A comparison of the buckling rotation strain curves of single-layer models comprising the finite-element models of Hudleston & Stephansson (1973) and Shimamoto & Hara (1976) with the experimental model of Hudleston (1973) is shown in Fig. 6(a)–(d) for viscosity ratios 100, 50, 30–24 and 10–11. The sets of curves show generally close agreement, especially for the maximum buckling rotation values. The highest discrepancies in % ε_s values corresponding to the peaks of curves (indicated by the arrows in Fig. 6) occur at the lowest viscosity ratios modelled (10–11), (Fig. 6d). Here, the maximum buckling rotation values for the experimental model occurs further to the right, at a higher bulk strain. The finite-element models are initiated with a low-amplitude fold of dominant wavelength whereas the experimental fold is not, and thus the position of the experimental curve probably reflects the amount of strain needed for the formation of the dominant wavelength fold.

The multilayer models of Williams (1980) have a viscosity ratio of 653 and are compared to the single-layer models of viscosity ratios of 1000 and 100 (Hudleston 1973) in Fig. 7. Although the curves have similar shapes, it can be seen that the peaks of the curves for similar strain values reach much higher values of buckling rotation in the multilayer model than in the single-layer model. The single-layer model can be thought of as a multilayer model in which the incompetent layer thickness is very large compared to that of the competent layer. Since the maximum buckling rotation value in the multilayer models decreases as thickness ratio increases, this suggests that, for a given viscosity ratio, there is an optimum thickness ratio at which buckling activity is at a maximum.

RELATIONSHIP BETWEEN BUCKLING ROTATION AND LAYER-PARALLEL SHORTENING

Hudleston (1973), Hudleston & Stephansson (1973) and Shimamoto & Hara (1976) also analysed layer-parallel shortening during folding for the buckle-fold models, using changes in arc length (length of the layer between fold-hinge points). Shimamoto & Hara (1976) found that the bulk of the layer-parallel shortening occurred up to limb dips of 15–20°, after which little shortening occurs and arc length was found to be almost constant after limb dips of 50–60°. Hudleston & Stephansson (1973) found that for a viscosity ratio of 10, arc length changed only slightly after 50–60% shortening (limb dips of 36–56°), while for a viscosity ratio of 100, shortening was markedly reduced after limb dips of 35°, and for a viscosity ratio of 1000, no detectable layer-parallel shortening occurred. In experimental studies, Hudleston (1973) noted that there was a marked slowing of arc length shortening after dips of 10–20° and after 20–30°, arc length was virtually constant. In Fig. 8, buckling rotation is plotted against limb dip, together with the above ranges in limb dip corresponding to most active layer-parallel shortening. For the models of Shimamoto & Hara (1976), the variation in initial limb dip for constant viscosity ratio was found to have little effect on the buckling rotation vs limb dip curves and

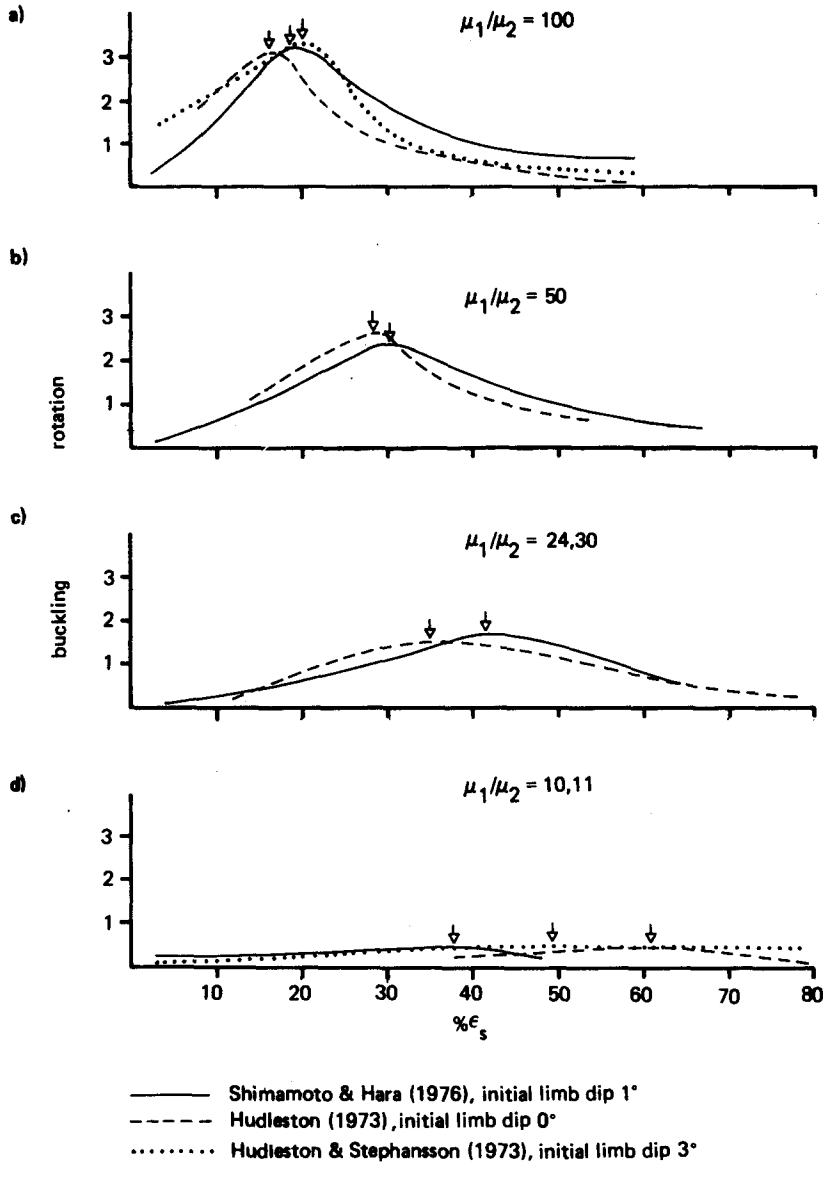

Fig. 6. Comparison of buckling rotation vs bulk strain curves from finite-element and experimental models of single-layer buckle folds. the curves agree best at higher viscosity ratios (μ_2/μ_2 = 100,50). At lower viscosity ratios (μ_1/μ_2 = 10, 11) the experimental model curve is displaced to the right. This is probably due to a delay in the experimental model caused by the development of the dominant wavelength fold which is already present at the start of deformation in the finite-element model.

thus only the averages of these have been plotted in Fig. 8(a).

In Fig. 8(a) & (b), showing the curves from the models of Shimamoto & Hara (1976) and Hudleston (1973), the range of limb dips marking the end of most active layer-parallel shortening coincides with the range of maximum values of buckling rotation. A similar relationship is evident in the model of Hudleston & Stephansson (1973) (Fig. 8c). For the model of viscosity ratio 100, the limb dip of the maximum buckling rotation value coincides with the limb dip at which layer-parallel shortening slows (35°). No layer-parallel shortening was detected for the viscosity ratio of 1000, and the buckling rotation vs limb dip curve shows that the maximum buckling rotation value occurs to the left of the first available value, i.e. within the first 2% ε_s deformation increment. For the lower viscosity ratio of 10, only small changes in arc length occurred after limb dips reached 36–56°.

Thus the data suggest that, for moderate to high viscosity ratios, the bulk of the layer-parallel shortening coincides with the initial rapid increase in buckling rotation and that it declines markedly when buckling rotation reaches a maximum. At low viscosity ratios, as in the case of the Hudleston & Stephansson's (1973) model for viscosity ratio of 10, the layer-parallel shortening is more likely to be controlled by the limb dip, which attained a high value before the maximum buckling rotation value was reached.

CONCLUSIONS

The rotation of a layer at any stage during buckle folding can be divided into two components: (a) the rotation which would occur due to pure shear if no competence contrast existed, termed 'pure shear rotation'; and (b) the additional rotation caused by the

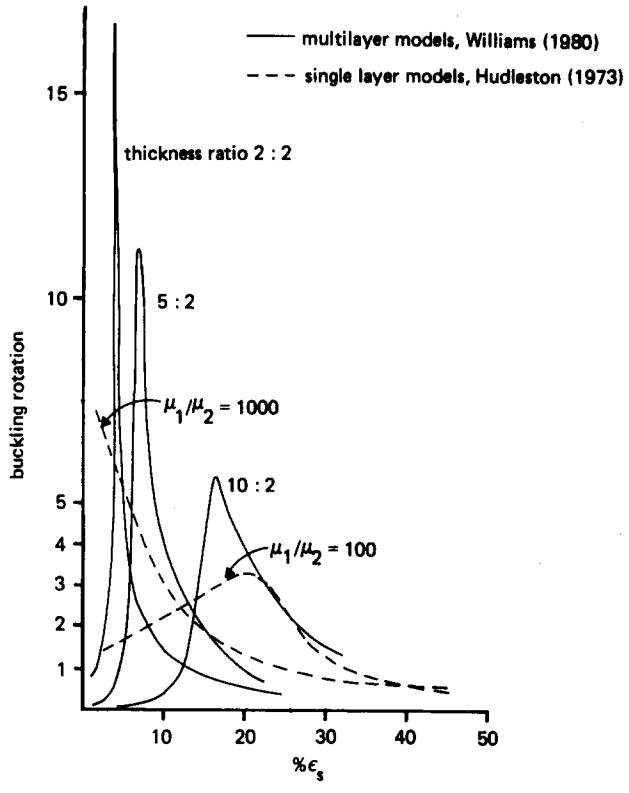

Fig. 7. Comparison of buckling rotation vs bulk strain curves from finite-element multilayer and single-layer buckle folds. The multilayer model folds (viscosity ratio 653) are compared to single-layer model folds of viscosity ratio 1000 and 100. The curves derived from the multilayer models show sharper peaks which reach higher values of buckling rotation than those of the single-layer models.

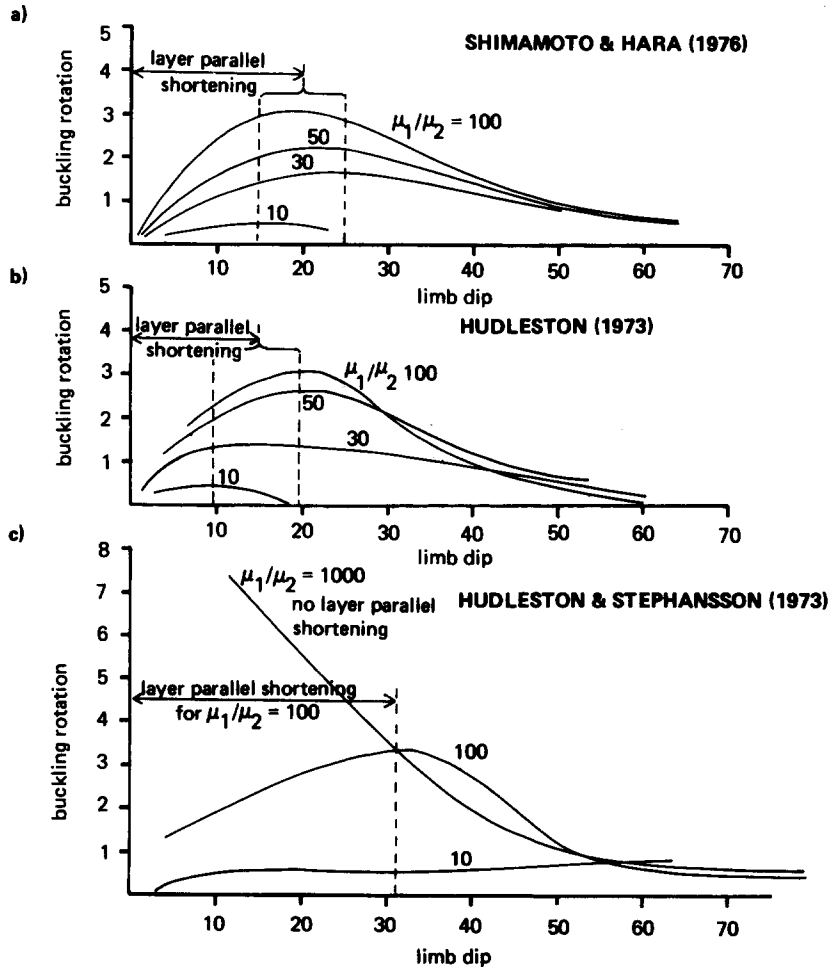

Fig. 8. Curves of buckling rotation vs limb dip for models of single-layer buckle folds. These show similar, skewed, bell-shaped curves to the buckling rotation vs strain curves. Also indicated on each plot is the range of most active layer-parallel shortening which coincides with the initial increase in buckling rotation. A sharp fall-off in layer-parallel shortening occurs when the buckling rotation reaches a maximum value.

competence contrast between the layer and its matrix, termed 'buckling rotation'. The 'buckling rotation' component provides a measure of buckling activity.

Four models of buckle folding were used to calculate buckling rotation vs strain. All produced skewed, bell-shaped curves. For single-layer models, the maximum value of buckling rotation and skewness of the curve increased with increasing viscosity ratio between the layer and its matrix. Models of multilayers showed similar shapes of curves in which the maximum buckling rotation value and degree of skewness decreased with increasing competent to incompetent layer thickness ratio, for a constant viscosity ratio. Comparison of the single-layer and multilayer curves suggests that for a given viscosity ratio, buckling activity is highest in the multilayer system. The period of most active layer-parallel shortening (decreasing arc length) occurs during the initial increase of buckling rotation; its wane coincides with the maximum buckling rotation.

The usual method of presenting fold growth in experimental and theoretical models is a plot of limb dip against strain. Such curves express the total cumulative rotation. By using the incremental rotation and separating it into 'pure shear' and 'buckling rotation' components, the variation in buckling activity becomes clearer. Curves of buckling rotation vs strain or limb dip could be used to compare different model results, to compare buckling activity to other variables during fold growth, such as layer-parallel shortening, or to check the behaviour of model materials. The method therefore provides a useful aid in the analysis of buckle fold modelling results.

Acknowledgements—The work presented in this paper was carried out while the author was employed at the Precambrian Research Unit, University of Cape Town, and forms part of a research project of the N.W. Cape subprogram of the National Geoscience Programme, supported financially by C.S.I.R. The author would like to thank Dr A. G. Milnes, Dr S. H. Treagus and two anonymous referees for critically reading the manuscript.

REFERENCES

Biot, M. A. 1957. Folding instability of a layered viscoelastic medium under compression. *Proc. R. Soc. Lond.* **A242**, 444–451.

Chapple, W. M. 1968. A mathematical theory of finite amplitude rock folding. *Bull. geol. Soc. Am.* **79**, 47–68.

Dieterich, J. H. & Carter, N. L. 1969. Stress-history of folding. *Am. J. Sci.* **267**, 129–154.

Hudleston, P. J. 1973. An analysis of 'single layer' folds developed in viscous media. *Tectonophysics* **16**, 189–214.

Hudleston, P. J. & Stephansson, O. 1973. Layer shortening and fold shape development in the buckling of single layer folds. *Tectonophysics* **17**, 299–322.

Ramberg, H. 1964. Selective buckling of composite layers with contrasted rheological properties, a theory for simultaneous formation of several orders of folds. *Tectonophysics* **1**, 307–341.

Ramsay, J. G. 1967. *Folding and Fracturing of Rocks*. McGraw-Hill, New York.

Shimamoto, T. & Hara, I. 1976. Geometry and strain distribution of single layer folds. *Tectonophysics* **19**, 271–289.

Williams, J. R. 1980. Similar and chevron folds in multilayers using finite-element and geometrical models. *Tectonophysics* **65**, 323–338.